scientific reports

Check for updates

OPEN

Soret and Dufour effects on a Casson nanofluid flow past a deformable cylinder with variable characteristics and Arrhenius activation energy

Naila Shaheen[1], Hashim M. Alshehri[2], Muhammad Ramzan[1], Zahir Shah[3]✉ & Poom Kumam[4,5]✉

In this study, the effects of variable characteristics amalgamated with chemical reaction and Arrhenius activation energy are analyzed on a two-dimensional (2D) electrically conducting radiative Casson nanoliquid flow past a deformable cylinder embedded in a porous medium. The surface of the cylinder is deformable in the radial direction i.e., the *z*-axis. The impression of Soret and Dufour's effects boosts the transmission of heat and mass. The flow is analyzed numerically with the combined impacts of momentum slip, convective heat, and mass conditions. A numerical solution for the system of the differential equations is attained by employing the bvp4c function in MATLAB. The dimensionless protuberant parameters are graphically illustrated and discussed for the involved profiles. It is perceived that on escalating the velocity slip parameter and porosity parameter velocity field depreciates. Also, on escalating the radiation parameter and heat transfer Biot number a prominent difference is noticed in an upsurge of the thermal field. For growing values of Brownian motion and thermophoretic parameters, temperature field augments. On escalating the curvature parameter and porosity parameter, drag force coefficient upsurges. The outcome of the Soret number, mass transfer Biot number, and activation energy parameter is quite eminent on the concentration distribution for the sheet in comparison to the deformable cylinder. A comparative analysis of the present investigation with an already published work is also added to substantiate the envisioned problem.

List of symbols

B_0	Magnetic field strength, A m^{-1}
$\tilde{C}$	Concentration of nanoparticles, kg m^{-3}
$\tilde{C}_w$	Concentration at the surface of the cylinder
$\tilde{C}_\infty$	Ambient concentration
c_s	Concentration susceptibility
c_p	Specific heat, m^2 s $^{-2}$ k^{-1}
C_f	Skin friction coefficient
D_B	Brownian diffusion coefficient

[1]Department of Computer Science, Bahria University, Islamabad 44000, Pakistan. [2]Department of Mathematics, Faculty of Science, King Abdulaziz University, Jeddah 21521, Saudi Arabia. [3]Department of Mathematical Sciences, University of Lakki Marwat, Lakki Marwat 28420, Khyber Pakhtunkhwa, Pakistan. [4]Fixed Point Research Laboratory, Fixed Point Theory and Applications Research Group, Center of Excellence in Theoretical and Computational Science (TaCS-CoE), Faculty of Science, King Mongkut's University of Technology Thonburi (KMUTT), 126 Pracha Uthit Rd., Bang Mod, Thung Khru, Bangkok 10140, Thailand. [5]Department of Medical Research, China Medical University Hospital, China Medical University, Taichung 40402, Taiwan. ✉email: zahir@ulm.edu.pk; poom.kum@kmutt.ac.th

D_T	Thermophoretic diffusion coefficient
$D_f = \frac{D_T k_t^* (\tilde{C}_w - \tilde{C}_\infty)}{\nu c_s c_p \left(\tilde{T}_w - \tilde{T}_\infty\right)}$	Dufour number
$D_B(C)$	Variable molecular diffusivity
d	Small parameter
E_a	Activation energy
$E = \frac{E_a}{k\tilde{T}_\infty}$	Activation energy parameter
e	Small parameter
$Ha = \frac{\sigma_1 B_0^2 l}{\rho U_1}$	Magnetic parameter
h_1	Convective heat transfer coefficient
h_2	Convective mass transfer coefficient
$H_1 = \frac{h_1}{k_\infty}\sqrt{\frac{\nu l}{U_1}}$	Heat transfer Biot number
$H_2 = \frac{h_2}{D_{B_\infty}}\sqrt{\frac{\nu l}{U_1}}$	Mass transfer Biot number
K^*	Permeability of porous medium
k_t^*	Thermal diffusion ratio
$k(T)$	Temperature-dependent thermal conductivity, W m^{-1} K^{-1}
k_r^2	Chemical reaction parameter
$\overline{k}$	Mean absorption coefficient
$L = S\sqrt{\frac{U_1}{\nu l}}$	Velocity slip parameter
l	Characteristic length
$N_b = \frac{\tau D_B (\tilde{C}_w - \tilde{C}_\infty)}{\nu}$	Brownian motion parameter
$N_t = \frac{\tau D_T \left(\tilde{T}_w - \tilde{T}_\infty\right)}{\nu \tilde{T}_\infty}$	Thermophoretic parameter
Nu_z	Local Nusselt number
$\Pr = \frac{\mu c_p}{k_\infty}$	Prandtl number
Q_1	Coefficient of heat generated or absorbed per unit volume
q_r	Radiative heat flux
$Q^* = \frac{Q_1 l}{\rho c_p U_1}$	Heat generation/absorption parameter
Q_w	Heat flux
Q_m	Mass flux
$\mathrm{Re}_z = \frac{U_1 z^2}{\nu l}$	Local Reynold number
$Rd = \frac{4\overline{\sigma}\tilde{T}_\infty^3}{\overline{k}k_\infty}$	Radiation parameter
S	Velocity slip factor
Sh_z	Local Sherwood number
$S_c = \frac{\nu}{D_B}$	Schmidt number
$S_r = \frac{D_T k_t^* \left(\tilde{T}_w - \tilde{T}_\infty\right)}{\nu \tilde{T}_\infty (\tilde{C}_w - \tilde{C}_\infty)}$	Soret number
Sh_z	Local Sherwood number
S	Velocity slip factor
$\tilde{T}$	Temperature, K
$\tilde{T}_w$	Temperature at the surface of the cylinder, K
$\tilde{T}_\infty$	Ambient temperature, K
$\tilde{u}, \tilde{w}$	Component of velocity in the direction of r&z
U_1	Reference velocity
r, z	Cylindrical polar coordinates
r-axis	Radial direction
z-axis	Axial direction
$W_w = \frac{U_1 z}{l}$	Velocity (stretching), m s^{-1}

Greek symbols

ν	Kinematic viscosity, m^2 s^{-1}
μ	Dynamic viscosity, Pa s
$\overline{\sigma}$	Stefan-Boltzmann coefficient, eVk^{-1}
σ_1	Electrical conductivity, s^3 m^2 kg^{-1}
ρ	Fluid density, kg m^{-3}
$\lambda = \frac{\nu l}{K^* U_1}$	Porosity parameter

$\delta = \frac{k_1^2 l}{U_1}$	Chemical reaction parameter
$\alpha = \frac{\tilde{T}_w - \tilde{T}_\infty}{\tilde{T}_\infty}$	Temperature difference
$\omega = \sqrt{\frac{\nu l}{U_1 R^2}}$	Curvature parameter
$\beta = \frac{\mu_c \sqrt{2\Pi_c}}{S_y}$	Casson parameter
ζ	Dimensionless parameter
τ_w	Shear stress at the surface

Researchers have immensely emphasized the transmission of heat past an elongated surface. It has enormous applications in the process of manufacturing, engineering, and industries such as continuous stretching of plastic sheets, aerodynamics, hot rolling, paper production, cooling of metallic plates, bar drawing, extrusion, and glass blowing. A numerical solution for time-independent two-phase Casson nanoliquid flow past a horizontal elongated cylinder is presented by Ramzan et al.[1]. The flow is incorporated with variable heat source/sink and Newtonian heating. It is found that the thermal field escalates for both phases for rising values of Newtonian heating. Reddy et al.[2] discussed the stagnation point flow of a radiative Eyring Powell liquid flow across an inclined stretchable cylinder. Buongiorno model is considered. Fluid flow is enhanced with an additional effect of Cattaneo Christov (CC) heat flux and chemical reaction. It is concluded that thermal and solutal field uplifts for rising values of curvature parameter. The upshot of homogeneous-heterogeneous reaction on an incompressible nanoliquid flow across a stretchable chamber is elucidated analytically and numerically by Sankar et al.[3]. It is observed that the thermal field boosts on amplifying the curvature parameter and Hartmann number. Mishra et al.[4] interpreted the influence of viscous dissipation combined with Ohmic dissipation on spherical and cylindrical-shaped nanoparticles over an elongated horizontal cylinder. It is witnessed that fluid flow accelerates for cylindrically shaped nanoparticles, however, a reverse trend is exhibited for spherical shaped nanoparticles. Consequently, exploration in this regard with different physical aspects can be seen in[5–15].

In the fluid flow, two mechanisms are involved in the conduction of heat. First, when the collision amid the molecules increases. Second, thermal conductivity plays a key role in escalating the random movement among the molecules. Thermal conductivity has significant applications in steam generators, electrolytes, concrete heating, and laminating. Abdelmalek et al.[16] numerically analyzed second-order velocity slip and bio convection on a pseudoplastic nanoliquid flow over a deformable cylinder. In this study transmission of heat and mass is communicated with the addition of temperature-dependent thermal conductivity and activation energy. The aftermath of temperature-dependent thermal conductivity and chemical reaction on a radiative Williamson nanoliquid is notified by Ibrahim et al.[17] past a horizontal stretchable cylinder immersed in a porous medium. The flow is incorporated with viscous dissipation and robin conditions. On a two-dimensional 2D radiative Non-Newtonian fluid flow past an extendable chamber is analytically demarcated by Raza et al.[18] alongside the influence of variable molecular diffusivity and temperature-dependent thermal conductivity. The Buongiorno model is utilized here. It is contemplated that thermal field enhances on mounting the Eckert number and radiation parameter, whereas, a decreasing output is noticed for fluid velocity on boosting the Reynold number. On a time-dependent, Maxwell fluid Khan et al.[19] numerically analyzed Cattaneo- Christov (CC) model over a deformable cylinder and sheet with variable thermal conductivity and mass diffusion. Further investigation on variable thermal conductivity across an elongated cylinder is mentioned in[20–25].

The Soret-Dufour factor plays a key role in the transmission of heat and mass on a moving fluid. It has a vital role in several applications which include the design of nuclear reactors, geothermal energy, groundwater pollutant migration, oil reservoirs, isotopes separation, manufacture of rubber and plastic sheets, the mixture of gases, compact heat insulation exchanger, and nuclear waste disposal. The features of the Soret and Dufour effect amalgamated with the chemical reaction on an MHD couple stress liquid are analytically addressed by Gajjela et al.[26] over an elongated cylinder. The findings disclosed that for growing values of curvature parameter thermal and solutal gradient upsurges. Tlili and Waqas[27] numerically analyzed the impact of bio convection and second-order slip on a radiative Oldroyd–B nanoliquid flow past a linear deformable cylinder. The flow is enhanced with the additional effect of zero mass flux and convective heat conditions. It is computed that fluid temperature upsurges by varying thermophoresis and curvature parameters. Radiative flux with Soret and Dufour effect on a second-grade fluid over an elongated cylinder is illustrated by Shojaei et al.[28]. It is perceived in this exploration that the solutal and thermal field tumbles on escalating the Schmidt number and Prandtl number. Using the Buongiorno model Jawad and Saeed[29] analytically explored the significance of the Soret Dufour factor on Maxwell fluid over a permeable elongated surface. The flow is incorporated with the addition of motile microorganisms and temperature-dependent thermal conductivity. It is reported that on mounting the Soret factor solutal field diminishes. Consequently, exploration in this regard with different physical aspects can be seen in refs.[30–43].

Researchers have manifested concern about fluid flow across the permeable surface. The flow through the porous chamber is very common and have widespread applications in industries, natural circumstances, petroleum, and chemical engineering for instance crude oil extraction, storage of nuclear waste material, movement of oil and water across the oil reservoir, heat exchangers, drying process, MHD generators, thermal insulation, seepage of water in river beds, filtration and water purification process. Singh et al.[44] investigated the combined influence of melting heat and variable heat source/sink with porosity effect across a horizontal stretchable cylinder. A numerical solution is obtained using the Keller box method. It is concluded that transmission of heat hikes on escalating the melting parameter, whereas, shear drag force diminishes for rising values of Reynold number. Bisht et al.[45] numerically studied the transmission of heat for Sisko nanoliquid in a porous medium across a linear deformable cylinder. It is found that transfer of heat declines on boosting the Brownian and porosity parameter, however, an uplift is noticed for the curvature parameter. Thermal features on a hybrid nanoliquid are analytically discussed by Saeed et al.[46] across a permeable elongated chamber. It is reported that fluid flow upsurges for rising values of curvature parameter. A reverse trend is observed in escalating the porosity parameter. The convective flow of hybrid nanoliquid in a porous medium through an elongated chamber is

Authors	Stretching cylinder	Soret Dufour effect	Temperature-dependent thermal conductivity	Thermal radiation	Variable molecular diffusivity	Porous medium	Activation energy
Reddy et al.[2]	Yes	No	No	Yes	No	No	Yes
Abdelmalek et al.[16]	Yes	No	Yes	No	No	No	Yes
Tulu et al.[21]	Yes	No	Yes	No	No	Yes	No
Tlili et al.[27]	Yes	No	No	Yes	No	No	Yes
Shojaei et al.[28]	Yes	Yes	No	Yes	No	No	No
Jagan et al.[42]	Yes	Yes	No	Yes	No	No	No
Present	Yes	Yes	Yes	Yes	Yes	Yes	Yes

Table 1. An inspection of literature for the innovation of the presented model.

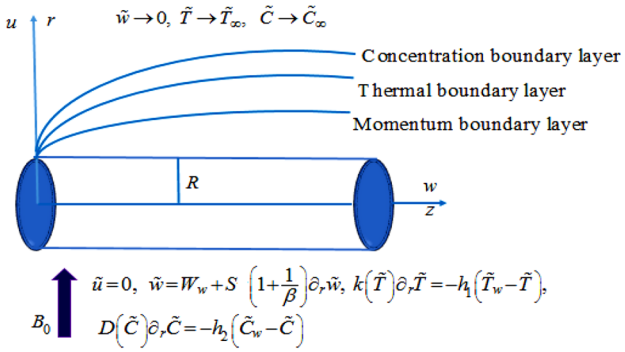

Figure 1. Flow representation of the model.

numerically explored by Aminian et al.[47]. It is revealed that enhancing the Hartman number rate of heat transfer escalates. Subsequently, exploration in this regard with different physical aspects can be seen in refs.[48–57].

According to the above-mentioned literature review, most of the researchers have investigated the characteristics of thermal radiation and activation energy past an elongated cylinder. The purpose of the present investigation is to examine the effect of temperature-dependent thermal conductivity, variable mass diffusion on a radiative Casson nanofluid flow past a deformable cylinder. The impression of the Soret and Dufour effect boosts the transmission of heat and mass. The flow is analyzed numerically with the combined impact of heat generation/absorption, chemical reaction with activation energy, momentum slip, and robin condition. The mathematical model is deciphered through MATLAB software bvp4c. The outcome of numerous parameters is examined for the deformable cylinder and stretching sheet via tabular and graphical illustrations. The uniqueness of the presented mathematical model is illustrated in Table 1 by associating it with the published studies.

Mathematical problem formulation. An incompressible, time-independent, 2D electrically conducting radiative Casson nanoliquid flow is examined past a deformable cylinder in a permeable medium. The nanoliquid model describes the attributes of Brownian motion and thermophoresis. The geometry of the problem is illustrated in cylindrical coordinate in such a manner that the cylinder is stretchable horizontally in the axial direction (i.e., z-axis) and the radial direction (i.e., r-axis) is orthogonal to it (Fig. 1). Transfer of heat and mass is enhanced with temperature-dependent thermal conductivity and variable molecular diffusivity incorporated with Soret and Dufour effect. Moreover, the impression of chemical reaction with activation energy, velocity slip effect, and robin conditions are analyzed.

The rheological equation for Casson fluid model is demarcated as[48,58]

$$\tau_{ij}=\begin{cases}\left(\mu_c+\frac{S_y}{(2\tilde{\pi})^{0.5}}\right)2\tilde{\gamma}_{ij}, & if\ \tilde{\pi}>\tilde{\pi}_c\\ \left(\mu_c+\frac{S_y}{(2\tilde{\pi}_c)^{0.5}}\right)2\tilde{\gamma}_{ij}, & if\ \tilde{\pi}<\tilde{\pi}_c\end{cases} \tag{1}$$

where τ_{ij} is the extra stress tensor and

$$\begin{aligned}&\tilde{\pi}=\tilde{\gamma}_{ij}\tilde{\gamma}_{ij}\ \text{is the product of the components of deformation rate}\\ &\tilde{\gamma}_{ij}=\frac{1}{2}\left(\partial_{x_j}v_i+\partial_{x_i}v_j\right)\ \text{is the rate of the strain tensor}\\ &\tilde{\pi}_c\ \text{is the critical value of deformation rate tensor}\\ &S_y\ \text{is the fluid yield stress.}\end{aligned} \tag{2}$$

The equations governing the flow[1,2,16,20,24] are as follows:

$$\partial_r(r\tilde{u})+\partial_z(r\tilde{w})=0, \tag{3}$$

$$\tilde{u}\partial_r\tilde{w}+\tilde{w}\partial_z\tilde{w}=\frac{\nu}{r}\left(1+\frac{1}{\beta}\right)\partial_r(r\partial_r\tilde{w})-\frac{\sigma_1 B_0^2}{\rho}\tilde{w}-\frac{\nu}{K^*}\tilde{w}, \tag{4}$$

$$\begin{aligned}\tilde{u}\partial_r\tilde{T}+\tilde{w}\partial_z\tilde{T}=&\frac{1}{\rho c_p}\frac{1}{r}\partial_r\left(k(T)r\partial_r\tilde{T}\right)+\tau\left(D_B\partial_r\tilde{T}\partial_r\tilde{C}+\frac{D_T}{\tilde{T}_\infty}\left(\partial_r\tilde{T}\right)^2\right)\\&-\frac{1}{\rho c_p}\frac{1}{r}\partial_r\left(r\partial_r q_r\right)+Q_1\frac{\left(\tilde{T}-\tilde{T}_\infty\right)}{\rho c_p}+\frac{D_T k_t^*}{c_s c_p}\frac{1}{r}\partial_r\left(r\partial_r\tilde{C}\right),\end{aligned} \tag{5}$$

$$\tilde{u}\partial_r\tilde{C}+\tilde{w}\partial_z\tilde{C}=\frac{1}{r}\partial_r\left(D_B\left(\tilde{C}\right)r\partial_r\tilde{C}\right)+\frac{D_T k_t^*}{\tilde{T}_\infty}\frac{1}{r}\partial_r\left(r\partial_r\tilde{T}\right)-k_r^2\left(\frac{\tilde{T}}{\tilde{T}_\infty}\right)\left(\tilde{C}-\tilde{C}_\infty\right)\exp\left(\frac{-E_a}{k\tilde{T}}\right). \tag{6}$$

The mathematical form of radiative heat flux[2] is as follows:

$$q_r=-\frac{4}{3}\frac{\overline{\sigma}}{\overline{k}}\partial_r T^4,\quad \text{where } T^4=4T_\infty^3T-3T_\infty^4 \tag{7}$$

In Eq. (5), temperature-dependent thermal conductivity[20] is stated as:

$$k(T)=k_\infty\left(1+d\left(\frac{\tilde{T}-\tilde{T}_\infty}{\tilde{T}_w-\tilde{T}_\infty}\right)\right) \tag{8}$$

In Eq. (6), variable molecular diffusivity[20] is expressed as:

$$D_B(C)=D_{B_\infty}\left(1+e\left(\frac{\tilde{C}-\tilde{C}_\infty}{\tilde{C}_w-\tilde{C}_\infty}\right)\right) \tag{9}$$

with boundary conditions[20,58]

$$\begin{aligned}&\tilde{u}|_{r=R}=0,\ \ \tilde{w}|_{r=R}=W_w+S\left(1+\frac{1}{\beta}\right)\partial_r\tilde{w},\ \ k(T)\partial_r\tilde{T}\Big|_{r=R}=-h_1\left(\tilde{T}_w-\tilde{T}\right),\\&D(C)\partial_r\tilde{C}\Big|_{r=R}=-h_2\left(\tilde{C}_w-\tilde{C}\right),\ \ \tilde{w}|_{r\to\infty}\to 0,\ \ \tilde{T}\Big|_{r\to\infty}\to\tilde{T}_\infty,\ \ \tilde{C}\Big|_{r\to\infty}\to\tilde{C}_\infty.\end{aligned} \tag{10}$$

Using appropriate subsequent transformation[24,59]

$$\begin{aligned}&\tilde{u}=-\frac{R}{r}.\left(\frac{\nu U_1}{l}\right)^{0.5}f(\zeta),\tilde{w}=\frac{U_1 z}{l}f'(\zeta),\zeta=-\left(\frac{U_1}{l\nu}\right)^{0.5}\left(\frac{R^2-r^2}{2R}\right),\\&\theta(\zeta)=\frac{\tilde{T}-\tilde{T}_\infty}{\tilde{T}_w-\tilde{T}_\infty},\phi(\zeta)=\frac{\tilde{C}-\tilde{C}_\infty}{\tilde{C}_w-\tilde{C}_\infty}.\end{aligned} \tag{11}$$

Utilizing transformation, Eq. (3) is trivially equated. Though Eqs. (4)–(6) and (10) are transmuted as:

$$\left(1+\frac{1}{\beta}\right)\left((1+2\omega\zeta)\frac{d^3f}{d\zeta^3}+2\omega\frac{d^2f}{d\zeta^2}\right)=f\frac{d^2f}{d\zeta^2}+\left(\frac{df}{d\zeta}\right)^2+(Ha+\lambda)\frac{df}{d\zeta}, \tag{12}$$

$$\begin{aligned}&(1+2\omega\zeta)\left((1+d\theta)+\frac{4}{3}Rd\right)\frac{d^2\theta}{d\zeta^2}=-2\omega\left((1+d\theta)+\frac{4}{3}Rd\right)\frac{d\theta}{d\zeta}\\&-\Pr\left(f\frac{d\theta}{d\zeta}+D_f\begin{pmatrix}2\omega\dfrac{d\phi}{d\zeta}\\+(1+2\omega\zeta)\dfrac{d^2\phi}{d\zeta^2}\end{pmatrix}+Q^*\theta\right)-(1+2\omega\zeta)\begin{pmatrix}d\left(\dfrac{d\theta}{d\zeta}\right)^2\\+\Pr\left(N_b\dfrac{d\theta}{d\zeta}\dfrac{d\phi}{d\zeta}+N_t\right)\left(\dfrac{d\theta}{d\zeta}\right)^2\end{pmatrix},\end{aligned} \tag{13}$$

$$(1+e\phi)(1+2\omega\zeta)\frac{d^2\phi}{d\zeta^2}=-\begin{pmatrix}2\omega(1+e\phi)\\+(1+2\omega\zeta)e\dfrac{d\phi}{d\zeta}\\+S_c f\end{pmatrix}\frac{d\phi}{d\zeta}-S_c\begin{pmatrix}S_r\begin{pmatrix}2\omega\dfrac{d\theta}{d\zeta}\\+(1+2\omega\zeta)\dfrac{d^2\theta}{d\zeta^2}\end{pmatrix}\\+\delta\phi(1+\alpha\theta)\exp\left(\dfrac{-E}{1+\alpha\theta}\right)\end{pmatrix}. \tag{14}$$

and the boundary conditions take the form:

$$f(\zeta)=0,\frac{df}{d\zeta}=1+L\left(1+\frac{1}{\beta}\right)\frac{d^2f}{d\zeta^2},\frac{d\theta}{d\zeta}=-H_1\left(\frac{1-\theta(0)}{1+d\theta}\right),\frac{d\theta}{d\zeta}=-H_2\left(\frac{1-\phi(0)}{1+e\phi}\right)\text{ at }\zeta=0$$

$$\frac{df}{d\zeta}\to 0,\frac{d\theta}{d\zeta}\to 0,\frac{d\phi}{d\zeta}\to 0\text{ as }\zeta\to\infty \tag{15}$$

The mathematical forms of shear stress at the wall (drag force coefficient), local Nusselt, and Sherwood number are specified as:

$$C_f=\frac{2\tau_w}{\rho W_w^2}\quad \tau_w=\mu\left(1+\frac{1}{\beta}\right)\partial_r\tilde{u}|_{r=R} \tag{16}$$

$$Nu_z=\frac{zQ_w}{k_\infty\left(\tilde{T}_w-\tilde{T}_\infty\right)}\quad Q_w=-k(T)\partial_r\tilde{T}+q_r\Big|_{r=R} \tag{17}$$

$$Sh_z=\frac{zQ_m}{D_{B_\infty}\left(\tilde{C}_w-\tilde{C}_\infty\right)}\quad Q_m=-D_B(C)\partial_r\tilde{C}\Big|_{r=R} \tag{18}$$

By employing Eq. (11), the dimensionless form of Eq. (16)–(18) are as follow:

$$\frac{1}{2}(\mathrm{Re}_z)^{0.5}C_f=\left(1+\frac{1}{\beta}\right)\frac{d^2f}{d\zeta^2}\Big|_{\zeta=0} \tag{19}$$

$$Nu_z(\mathrm{Re}_z)^{-0.5}=-\left(1+\frac{4}{3}\left(\frac{Rd}{1+d\theta}\right)\right)\frac{d\theta}{d\zeta}\Big|_{\zeta=0} \tag{20}$$

$$Sh_z(\mathrm{Re}_z)^{-0.5}=-(1+e\phi)\frac{d\phi}{d\zeta}\Big|_{\zeta=0} \tag{21}$$

Numerical procedure

The solution of the system of highly nonlinear differential equations can be obtained by numerous analytical, exact, and numerical procedures[10,13,56,60–71]. The proposed mathematical model is handled numerically. Here, the coupled nonlinear ODEs are computed numerically by employing the bvp4c function in MATLAB. Mentioned numerical code is used, we obtain ODEs which are of order one.

$$f=Y_1,f'=Y_2,f''=Y_3,f'''=Y_3'=YY_1,$$

$$YY_1=\left(\left(\frac{1}{1+\frac{1}{\beta}}\right)\left(\frac{1}{1+2\omega\zeta}\right)\right)\left(Y_1.Y_3+Y_2^2+(Ha+\lambda)Y_2\right)-\left(\frac{2\omega}{1+2\omega\zeta}\right)Y_3,$$

$$\theta=Y_4,\theta'=Y_5,\theta''=Y_5'=YY_2,$$

$$\phi=Y_6,\phi'=Y_7,\phi''=Y_7'=YY_3.$$

$$YY_2=\left(\frac{1}{(1+2\omega\zeta)\left((1+d.Y_4)+\frac{4}{3}Rd\right)}\right)\begin{pmatrix}-\left((1+2\omega\zeta)d.Y_5+2\omega\left((1+d.Y_4)+\frac{4}{3}Rd\right)\right)Y_5\\-\Pr\,(1+2\omega\zeta)\left(N_bY_5.Y_7+N_tY_5^2\right)\\-\Pr\left(2\omega.D_f.Y_7+f.Y_5+Q^*.Y_4+D_f(1+2\omega\zeta).YY_3\right)\end{pmatrix},$$

$$YY_3=\left(\frac{1}{(1+e.Y_6)(1+2\omega\zeta)}\right)\begin{pmatrix}-(e.Y_7.(1+2\omega\zeta)+2\omega(1+e.Y_6))Y_7\\-S_c\begin{pmatrix}Y_1.Y_7+S_r(2\omega.Y_5+(1+2\omega\zeta).YY_2)\\+\delta.Y_6(1+\alpha.Y_4)^n\exp\left(\frac{-E}{1+\alpha.Y_4}\right)\end{pmatrix}\end{pmatrix}.$$

and the boundary conditions are enumerated as

$$Y_1(0)=0,Y_2(0)=1+L\left(1+\frac{1}{\beta}\right)Y_3(0),Y_5(0)=-H_1\left(\frac{1-Y_4(0)}{1+d.Y_4(0)}\right),Y_7(0)=-H_2\left(\frac{1-Y_6(0)}{1+e.Y_6(0)}\right),\quad\text{at}\quad\zeta=0$$

$$Y_2(\infty)\to 0,Y_4(\infty)\to 0,Y_6(\infty)\to 0.\text{ as }\zeta\to\infty \tag{22}$$

Analysis of results

For the graphical analysis of the dimensionless parameters versus involved profiles appearing in the highly nonlinear mathematical problem in Eqs. (12)–(15). This problem is elucidated numerically by utilizing bvp4c, an implemented function in MATLAB. The impression of sundry on the velocity of the fluid, transmission of heat, and mass are shown graphically in such a manner that solid lines correspond to a deformable cylinder and

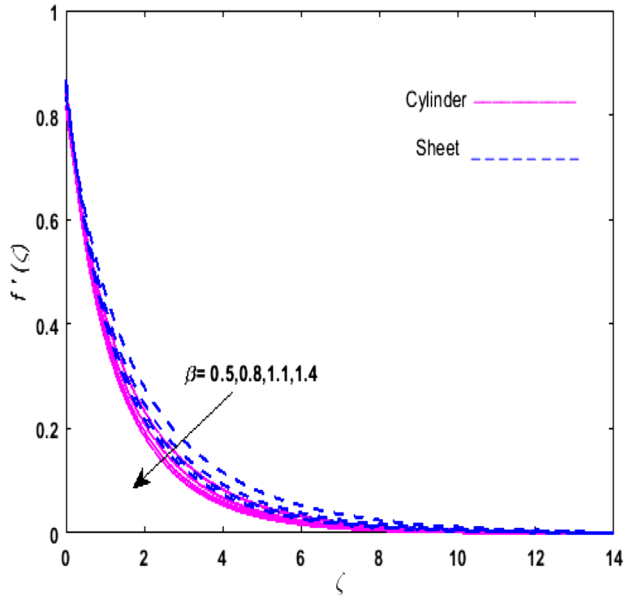

Figure 2. Upshot of β on $f'(\zeta)$.

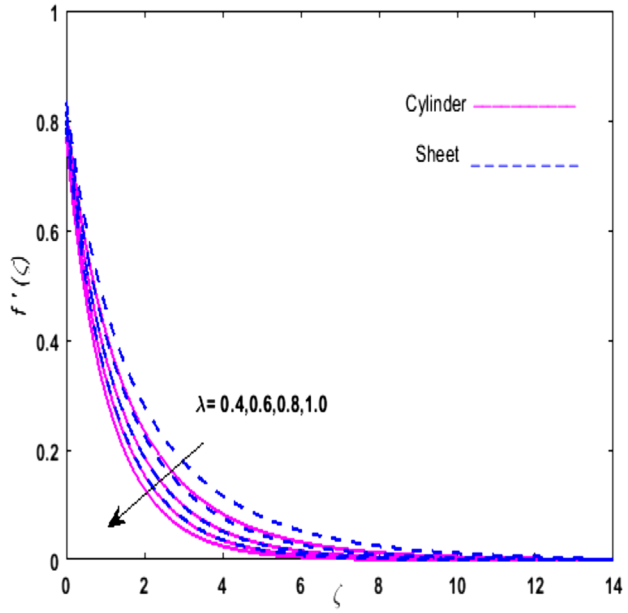

Figure 3. Upshot of λ on $f'(\zeta)$.

dotted lines for the case of deformable surface which are portrayed in Figs. 2, 3, 4, 5, 6, 7, 8, 9, 10, 11, 12, 13, 14, 15, 16 and 17. Figures 2, 3, 4, 5 and 6 demonstrate the influence of the Casson fluid parameter β, velocity slip parameter L, porosity parameter λ, curvature parameter ω, and magnetic parameter Ha on the velocity of the fluid $f'(\zeta)$. The aftermath of β on velocity field is illustrated in Fig. 2. As β is inversely proportional to yield stress S_y. It is found that on escalating β yield stress decreases. This generates a resistive force that causes hindrance to the fluid flow. Consequently, a decreasing trend is perceived in the $f'(\zeta)$ for both the stretchable cylinder and deforming sheet. The variation of the porosity parameter λ on the fluid flow is presented in Fig. 3. Since λ is the quotient of kinematic viscosity to the permeability of the porous medium. Growing values of λ escalates the kinematic viscosity of the fluid. This accelerates the resistance in the system. It is found that on elevating λ a deterrence is witnessed to the motion of the fluid. Due to mounting values of λ, sponginess in the medium reduces. Hence, $f'(\zeta)$ diminishes for both the cylinder and the sheet. The impact of the velocity slip parameter L on $f'(\zeta)$ is sketched in Fig. 4. As growing values of L strengthens the friction force. Thus, more liquid slips past the deforming cylinder. Therefore, fluid velocity depreciates in both cases for rising values of L. Hence, the behavior of the curvature parameter ω on the fluid flow is represented in Fig. 5. It is noticed that on uplifting the

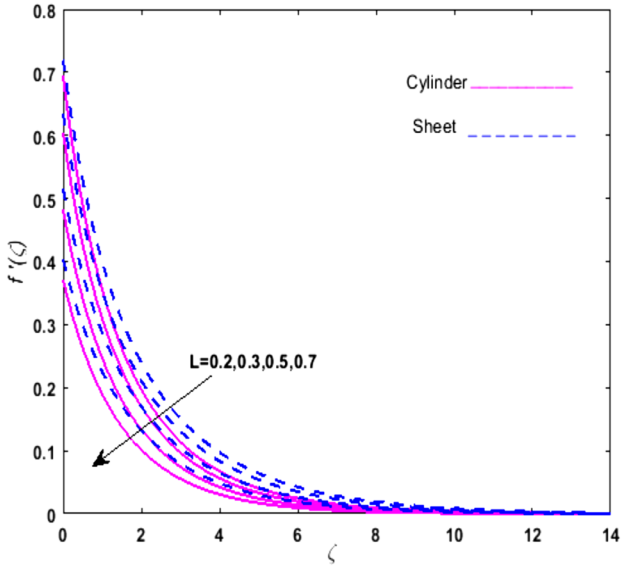

Figure 4. Upshot of L on $f'(\zeta)$.

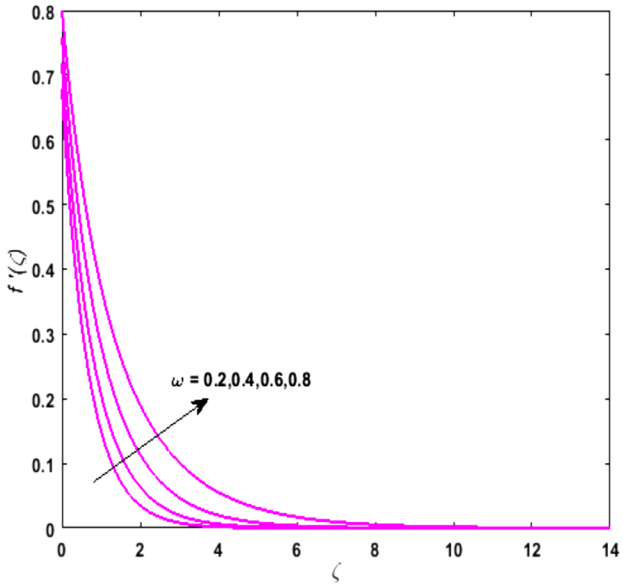

Figure 5. Upshot of ω on $f'(\zeta)$.

ω, the radius of the stretching cylinder depreciates. Thus, resistivity in the fluid accelerates near the surface, whereas, far away from the stretching cylinder deterrence in the fluid declines. Therefore, $f'(\zeta)$ augments. Figure 6 reflects the comportment of magnetic parameter Ha on $f'(\zeta)$. Rising values of Ha strengthens the Lorentz force. Due to which resistance arises between the fluid and the surface. Consequently, flow over the deformable cylinder slows down. Therefore, a downfall is noticed in $f'(\zeta)$ on enhancing the magnetic parameter. The outcome of the heat transfer Biot number H_1 on the temperature field $\theta(\zeta)$ is revealed in Fig. 7. Heat transfer coefficient upsurges on uplifting H_1. Due to which more heat is transmitted from the heated stretchable cylinder to the liquid. Hence, $\theta(\zeta)$ boosts for both cases. A prominent difference is noticed in an upsurge of temperature for the flat surface. On the other hand, the impact of temperature has a larger effect on the deformable cylinder. To elaborate the impression of the thermophoresis parameter N_t on $\theta(\zeta)$ is mapped in Fig. 8. It is noticed that on enhancing N_t, thermophoretic force is strengthened. As a result, fluid particles move from the heated liquid to the cold fluid. Hence, enhancement in $\theta(\zeta)$ is prominent for both the deformable cylinder and the flat sheet. Figure 9 illustrates the impression of the Brownian motion parameter N_b on $\theta(\zeta)$. For growing values of N_b collision among the fluid particles increases due to which more heat is generated. Therefore, $\theta(\zeta)$ rises. The aftermath of temperature is elevated as well as enduring for both N_t and N_b for deformable sheet. Figure 10 displays the

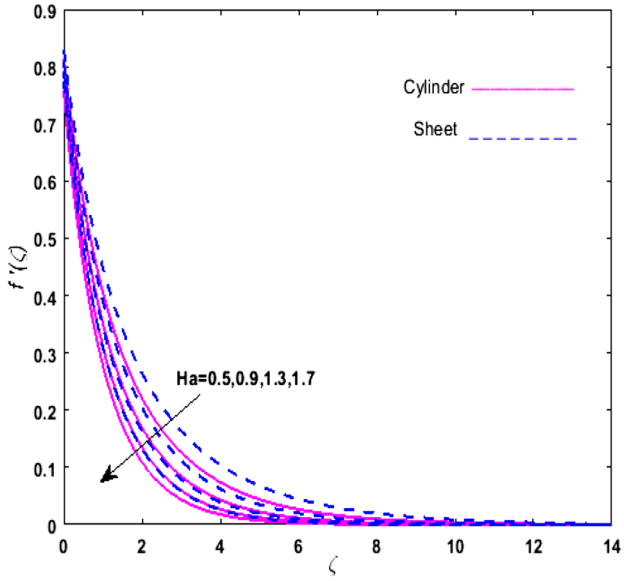

Figure 6. Upshot of Ha on $f'(\zeta)$.

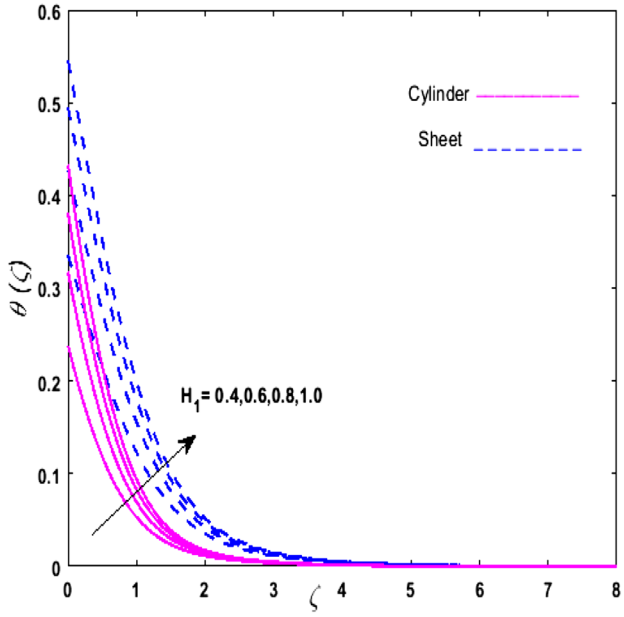

Figure 7. Upshot of H_1 on $\theta(\zeta)$.

outcome of the radiation parameter Rd on $\theta(\zeta)$. Since $Rd = \frac{4\bar{\sigma}T_\infty^3}{3\bar{k}k}$, so by escalating Rd the mean absorption coefficient decreases. Therefore, due to growing values of Rd more heat is transmitted to the fluid. Hence, $\theta(\zeta)$ rises. However, elevation in the temperature of the fluid for the stretching surface is eminent as well as lasting. The performance of heat generation and absorption parameter Q^* on $\theta(\zeta)$ is addressed in Fig. 11a, b. It is seen that on amplifying Q^* huge amount of heat is generated. Thus, more heat is added to the system. Hence, the thermal field upsurges, whereas, negative values of Q^* less amount of heat is generated. Consequently, the thermal field deteriorates. It is perceived that temperature rise is rapid for both the cylinder and the sheet. However, it is noted that the temperature of the deformable cylinder is lower than the sheet as well as enduring far away from the surface. To understand the variation of the Dufour number D_f on $\theta(\zeta)$ Fig. 12 is plotted. On escalating D_f concentration gradient enhances, whereas, temperature gradient decreases which results in heat transmission. Thus, a prominent upsurge is found in the thermal state of $\theta(\zeta)$ which is quite eminent for the stretching sheet. The impression of the Schmidt number S_c on the concentration profile $\phi(\zeta)$ is portrayed in Fig. 13. As S_c is the quotient of kinematic viscosity ν to Brownian diffusion coefficient D_B. It is noticed that mass diffusion diminishes

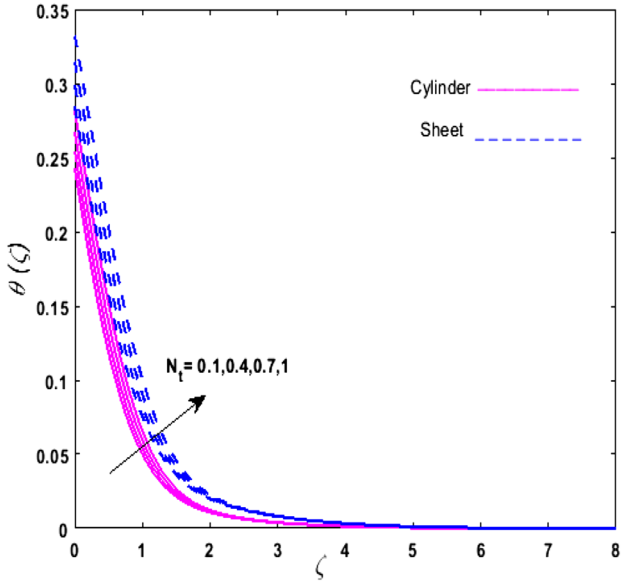

Figure 8. Upshot of N_t on $\theta(\zeta)$.

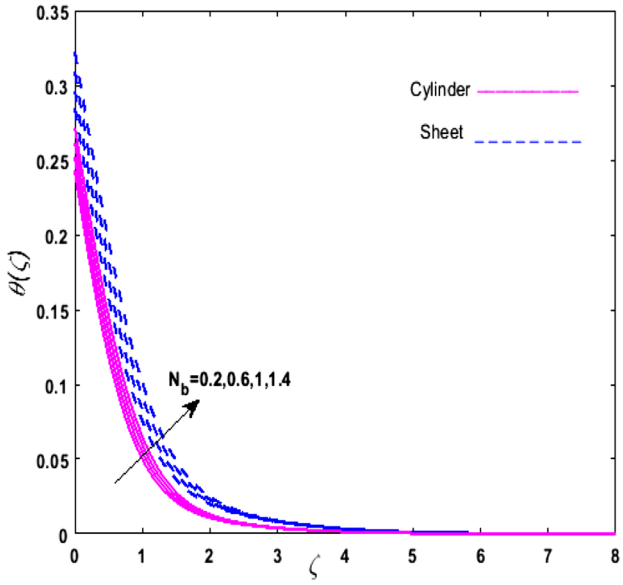

Figure 9. Upshot of N_b on $\theta(\zeta)$.

for growing values of S_c. This results in the reduction of the concentration of the fluid. Therefore, deteriorating nature is exhibited by $\phi(\zeta)$ on boosting S_c. Figure 14 is drawn to elucidate the upshot of dimensionless chemical reaction parameter δ on $\phi(\zeta)$. On up surging δ, chemical molecular diffusivity reduces owing to its consumption in the reaction. Hence, it is observed that on boosting δ concentration field deteriorates. It is witnessed that the aftermath of concentration on the stretchable cylinder is much lower and long-lasting on escalating S_c and δ. Figure 15 is sketched to analyze the effect of Soret number S_r on $\phi(\zeta)$. S_r is the quotient of temperature difference to concentration. On escalating S_r, the temperature gradient rises. It is perceived that molecular diffusion increases. Thus, the rate of mass transfer intensifies for growing values of S_r. Consequently, $\phi(\zeta)$ enhances.

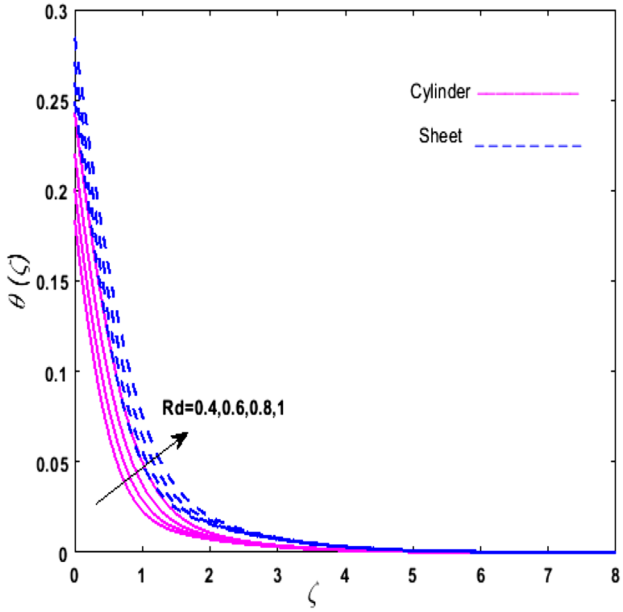

Figure 10. Upshot of Rd on $\theta(\zeta)$.

Figure 16 is plotted to understand the features of mass transfer Biot number H_2. It is perceived that H_2 depends on the mass transfer coefficient h_2. Therefore, growing values of H_2 elevates $\phi(\zeta)$. The impression of mounting values of activation energy E is deliberated in Fig. 17. It is noticed that escalating values of E lead to a decrease in the Arrhenius function. Consequently, the generative chemical reaction decelerates. Thus, on escalating E, the fluid concentration upsurges. It is found that concentration distribution on augmenting S_r, H_2 and E is quite eminent for sheet in comparison to the deformable cylinder. The outcome of tabulated values of dimensionless parameters ω, λ, Ha and L. on drag force coefficient is depicted in Table 2. It is perceived that on escalating ω, λ and Ha shear stress increases, however, a reverse upshot is seen on mounting L. The influence of Pr, H_1, D_f, H_2, S_r, N_b, S_c and N_t on local Nusselt number and Sherwood number is portrayed in Table 3. It is perceived that on escalating D_f, H_2, S_r, N_b, S_c and N_t mass flux augments, whereas, heat flux diminishes. A deteriorating nature is exhibited by mass transfer on amplifying Pr and H_1, however, the rate of heat transfer amplifies. A comparative analysis of the present investigation is exhibited in Table 4 with Fathizadeh et al.[72], Fang et al.[73], and Imtiaz et al.[74]. A good association between theresults is seen.

Concluding remarks

The numerical solution for radiative Casson nanofluid flow with variable characteristics incorporated with chemical reaction and Arrhenius activation energy has been obtained past a deformable cylinder. Transfer of heat and mass is enhanced by inspecting the impression of the Soret-Dufour factor with robin conditions. The mathematical model is deciphered through bvp4c, an implemented function in MATLAB. Graphical impressions of the parameters involved in the mathematical problem are illustrated for the deformable cylinder and stretching sheet. The perceptible analyses of the present investigation are:

- A decreasing trend is noticed in the velocity field for fluctuation in the Casson fluid parameter, velocity slip parameter, and porosity parameter.
- The thermal field amplifies escalating Rd.
- For growing values of N_t and N_b temperature field augments.
- On elevating the heat transfer Biot number a prominent difference is noticed in the upsurge of temperature for the flat sheet.
- For larger values of S_c and δ the concentration field declines.
- The outcome of augmenting S_r, H_2 and E is quite eminent on the concentration distribution for the sheet in comparison to the deformable cylinder.
- Drag force coefficient increases on escalating ω, λ and Ha
- The mass transfer exhibits a deteriorating impact on amplifying Pr and H_1, however, the rate of heat transfer amplifies.
- Mass flux augments on escalating D_f, N_b, S_c and N_t.

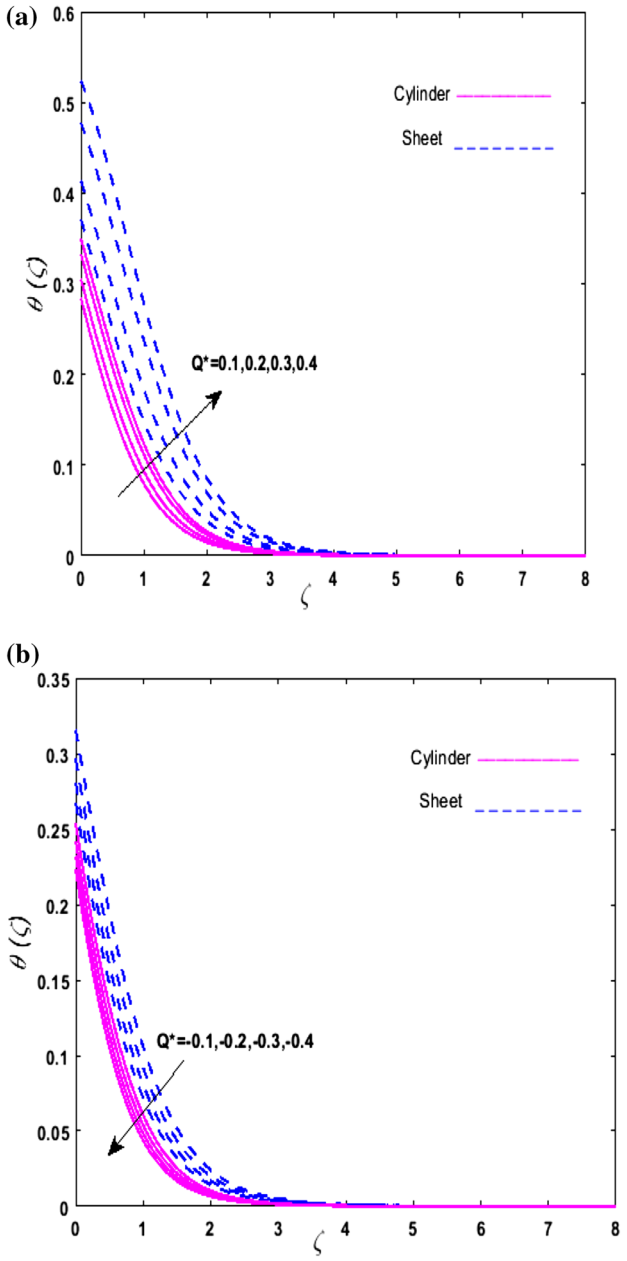

Figure 11. Upshot of (**a**) $(Q* > 0)$ on $\theta(\zeta)$, (**b**) $(Q* < 0)$ on $\theta(\zeta)$.

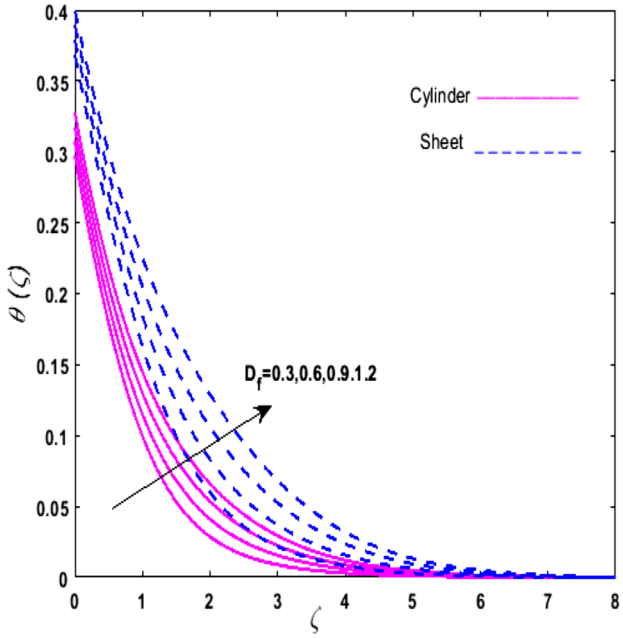

Figure 12. Upshot of D_f on $\theta(\zeta)$.

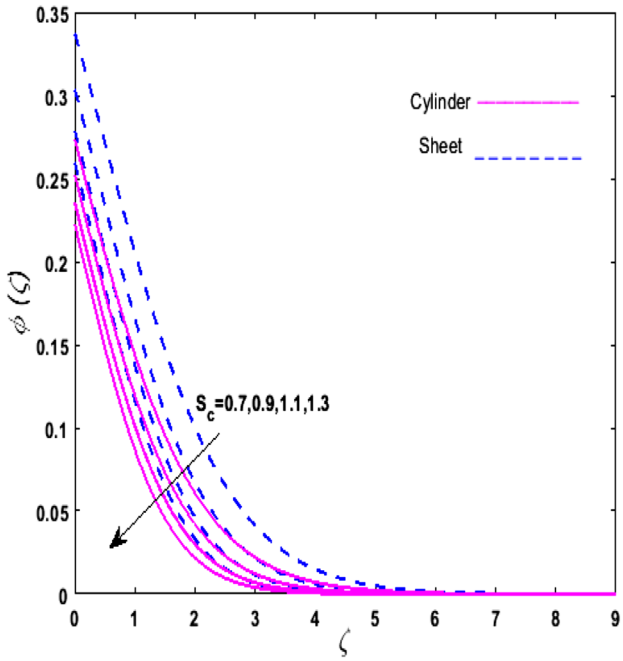

Figure 13. Upshot of S_c on $\phi(\zeta)$.

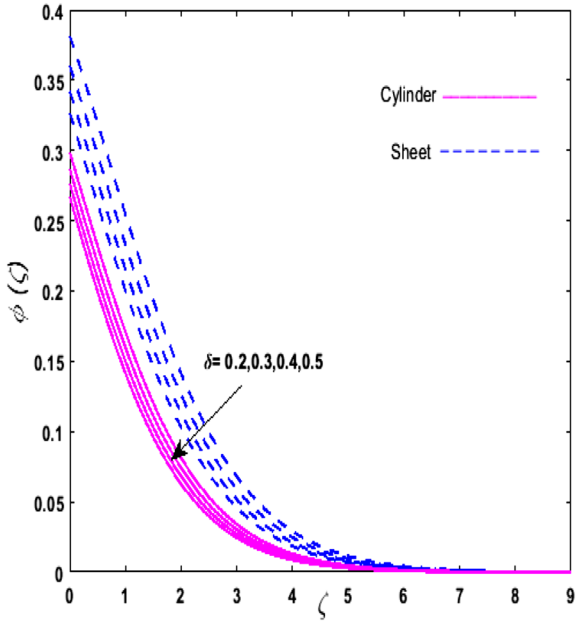

Figure 14. Upshot of δ on $\phi(\zeta)$.

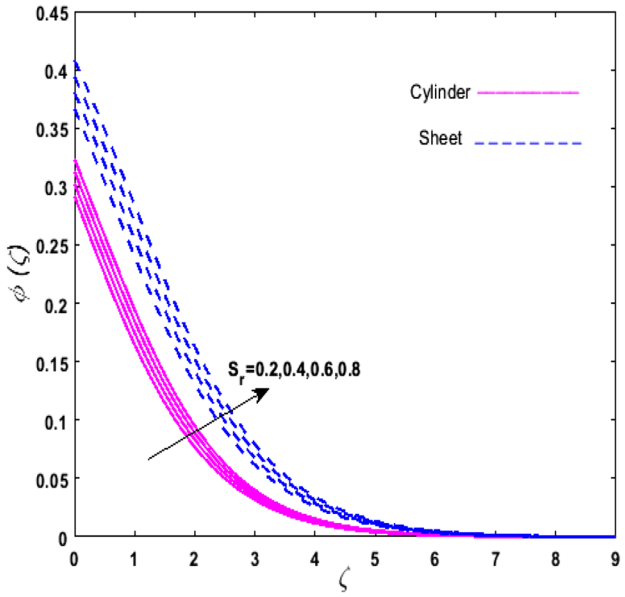

Figure 15. Upshot of S_r on $\phi(\zeta)$.

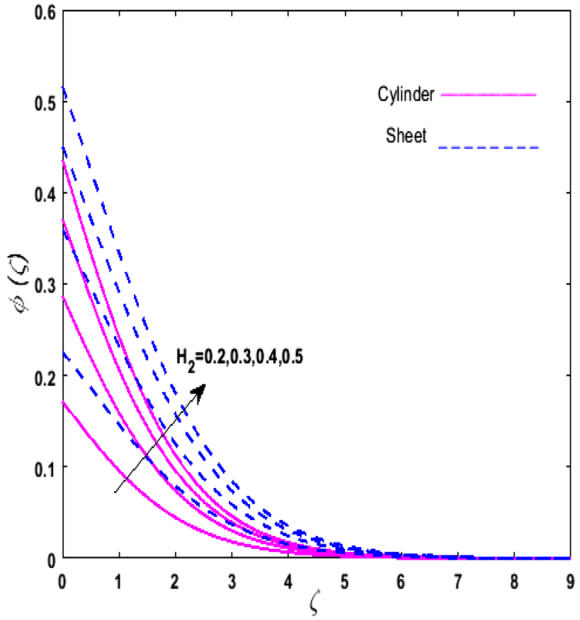

Figure 16. Upshot of H_2 on $\phi(\zeta)$.

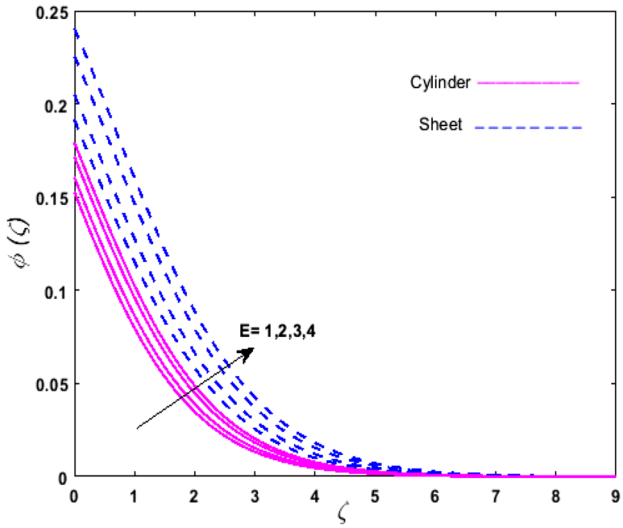

Figure 17. Upshot of E on $\phi(\zeta)$.

ω	λ	Ha	L	$-\left(1+\frac{1}{\beta}\right)\frac{d^2f}{d\zeta^2}\Big\vert_{\zeta=0}$
0.1				1.4510035
0.2				1.6070220
0.3				1.7807451
	0.4			1.5589928
	0.5			1.6088920
	0.6			1.6564151
		0.3		1.3923086
		0.5		1.5064596
		0.7		1.6088920
			0.3	1.0010071
			0.4	0.9841995
			0.5	0.8913582

Table 2. Computationalvalues of friction drag coefficient for distinct values of ω, λ, Ha and L.

Pr	H_1	D_f	H_2	S_r	N_b	S_c	N_t	$Nu_z(\mathrm{Re}_z)^{-0.5}$	$Sh_z(\mathrm{Re}_z)^{-0.5}$
4								0.4647132	0.07975943
6								0.4833629	0.07957307
8								0.4955689	0.07944563
	0.1							0.1441683	0.08233553
	0.3							0.3834158	0.08041072
	0.5							0.5727355	0.07880583
		0.3						0.4911270	0.07960337
		0.5						0.4812924	0.07966677
		0.7						0.4710714	0.07973468
			0.1					0.4959289	0.07957307
			0.3					0.4874835	0.17771861
			0.5					0.4828872	0.23514202
				0.2				0.4900239	0.06330082
				0.4				0.4766769	0.06918812
				0.6				0.4602900	0.07594917
					0.1			0.4978845	0.07957307
					0.3			0.4939279	0.07962442
					0.5			0.4897862	0.07967779
						0.6		0.4986354	0.07806048
						0.8		0.4959289	0.07957309
						1		0.4932983	0.08065435
							0.2	0.4969961	0.07958369
							0.4	0.4951655	0.079610632
							0.6	0.4932593	0.079636848

Table 3. Computational values of $Nu_z(\mathrm{Re}_z)^{-0.5}$ and $Sh_z(\mathrm{Re}_z)^{-0.5}$ against the different estimation of $\mathrm{Pr}, H_1, D_f, H_2, S_r, N_b, S_c$ and N_t.

	Present	Fathizadeh[72]			Fang[73]	Imtiaz[74]
Ha	bvp4c	HPM	M-HPM	Exact solution	Exact solution	HAM
0	− 1	− 1	− 1	− 1	− 1	− 1
0.5	− 1.11825	–	–	–	− 1.1180	− 1.1180
1	− 1.41421	− 1.41421	− 1.41421	− 1.41421	–	− 1.4142
5	− 2.44943	− 2.44948	− 2.44948	− 2.44948	–	− 2.4494
10	− 3.31626	− 3.31662	− 3.31662	− 3.31662	–	–

Table 4. Comparison of $f''(0)$ when $\omega = \lambda = \Pr = d = Rd = N_t = N_b = Q^* = D_f = e = S_c = \delta = \alpha = E = L = H_1 = H_2 = 0, \beta \to \infty$ with Fathizadeh et al.[72], Fang et al.[73], and Imtiaz et al.[74] with the present work.

Received: 10 April 2021; Accepted: 8 September 2021
Published online: 29 September 2021

References

1. Ramzan, M. *et al.* Impact of Newtonian heating and Fourier and Fick's laws on a magnetohydrodynamic dusty Casson nanofluid flow with variable heat source/sink over a stretching cylinder. *Sci. Rep.* **11**(1), 1–19 (2021).
2. Reddy, S. R. R., Reddy, P. B. A. & Rashad, A. M. Activation energy impact on chemically reacting Eyring-Powell Nanofluid flow over a stretching cylinder. *Arab. J. Sci. Eng.* **45**, 5227–5242 (2020).
3. Sankar Giri, S., Das, K. & Kundu, P. K. Homogeneous–heterogeneous reaction mechanism on MHD carbon nanotube flow over a stretching cylinder with prescribed heat flux using differential transform method. *J. Comput. Des. Eng.* **7**(3), 337–351 (2020).
4. Mishra, A. & Kumar, M. Velocity and thermal slip effects on MHD nanofluid flow past a stretching cylinder with viscous dissipation and Joule heating. *SN Appl. Sci.* **2**(8), 1–13 (2020).
5. Sohail, M. & Naz, R. Modified heat and mass transmission models in the magnetohydrodynamic flow of Sutterby nanofluid in stretching cylinder. *Physica A Stat. Mech. Appl.* **549**, 124088 (2020).
6. Ramzan, M., Sheikholeslami, M., Chung, J. D. & Shafee, A. Melting heat transfer and entropy optimization owing to carbon nanotubes suspended Casson nanoliquid flow past a swirling cylinder-A numerical treatment. *AIP Adv.* **8**(11), 115130 (2018).
7. Liu, C. *et al.* Nonlinear radiative Maxwell nanofluid flow in a Darcy–Forchheimer permeable media over a stretching cylinder with chemical reaction and bioconvection. *Sci. Rep.* **11**(1), 1–21 (2021).
8. Samrat, S. P., Reddy, M. G. & Sandeep, N. Buoyancy effect on magnetohydrodynamic radiative flow of Casson fluid with Brownian moment and thermophoresis. *Eur. Phys. J. Spec. Top.* **230**, 1273–1281 (2021).
9. Alwawi, F. A., Alkasasbeh, H. T., Rashad, A. M. & Idris, R. Heat transfer analysis of ethylene glycol-based Casson nanofluid around a horizontal circular cylinder with MHD effect. *Proc. Inst. Mech. Eng. C J. Mech. Eng. Sci.* **234**(13), 2569–2580 (2020).
10. Ibrahim, M. & Khan, M. I. Mathematical modeling and analysis of SWCNT-Water and MWCNT-Water flow over a stretchable sheet. *Comput. Methods Programs Biomed.* **187**, 105222 (2020).
11. Ramzan, M., Gul, H. & Chung, J. D. Double stratified radiative Jeffery magneto nanofluid flow along an inclined stretched cylinder with chemical reaction and slip condition. *Eur. Phys. J. Plus* **132**(11), 1–17 (2017).
12. Reddy, G. J., Kethireddy, B., Kumar, M. & Rani, H. P. Entropy generation for transient Casson fluid past a vertical cylinder with Bejan's flow visualization. *Int. J. Comput. Methods Eng. Sci. Mech.* **20**(3), 175–200 (2019).
13. Muhammad, R., Khan, M. I., Khan, N. B. & Jameel, M. Magnetohydrodynamics (MHD) radiated nanomaterial viscous material flow by a curved surface with second order slip and entropy generation. *Comput. Methods Programs Biomed.* **189**, 105294 (2020).
14. Alamri, S. Z., Khan, A. A., Azeez, M. & Ellahi, R. Effects of mass transfer on MHD second grade fluid towards stretching cylinder: A novel perspective of Cattaneo-Christov heat flux model. *Phys. Lett. A* **383**(2–3), 276–281 (2019).
15. Ramzan, M., Bilal, M. & Chung, J. D. Radiative flow of Powell-Eyring magneto-nanofluid over a stretching cylinder with chemical reaction and double stratification near a stagnation point. *PLoS ONE* **12**(1), e0170790 (2017).
16. Abdelmalek, Z. *et al.* A mathematical model for bioconvection flow of Williamson nanofluid over a stretching cylinder featuring variable thermal conductivity, activation energy and second-order slip. *J. Thermal Anal. Calorim.* **144**, 205–217 (2021).
17. Ibrahim, W. & Negera, M. Viscous dissipation effect on mixed convective heat transfer of MHD flow of Williamson nanofluid over a stretching cylinder in the presence of variable thermal conductivity and chemical reaction. *Heat Transf.* **50**(3), 2427–2453 (2021).
18. Raza, R., Sohail, M., Abdeljawad, T., Naz, R. & Thounthong, P. Exploration of temperature-dependent thermal conductivity and diffusion coefficient for thermal and mass transportation in sutterby nanofluid model over a stretching cylinder. *Complexity* **2021**, 6252864 (2021).
19. Khan, M., Ahmed, A., Irfan, M. & Ahmed, J. Analysis of Cattaneo-Christov theory for unsteady flow of Maxwell fluid over stretching cylinder. *J. Therm. Anal. Calorim.* **144**, 145–154 (2020).
20. Waqas, H., Manzoor, U., Shah, Z., Arif, M. & Shutaywi, M. Magneto-burgers nanofluid stratified flow with swimming motile microorganisms and dual variables conductivity configured by a stretching cylinder/plate. *Math. Probl Eng.* **2021**, 8817435 (2021).
21. Tulu, A. & Ibrahim, W. Spectral relaxation method analysis of Casson nanofluid flow over stretching cylinder with variable thermal conductivity and Cattaneo–Christov heat flux model. *Heat Transf.* **49**(6), 3433–3455 (2020).
22. Samrat, S. P., Sulochana, C. & Ashwinkumar, G. P. Impact of thermal radiation on an unsteady Casson nanofluid flow over a stretching surface. *Int. J. Appl. Comput. Math.* **5**(2), 1–20 (2019).
23. Alwawi, F. A., Alkasasbeh, H. T., Rashad, A. M. & Idris, R. MHD natural convection of Sodium Alginate Casson nanofluid over a solid sphere. *Results Phys.* **16**, 102818 (2020).
24. Aziz, A. & Shams, M. Entropy generation in MHD Maxwell nanofluid flow with variable thermal conductivity, thermal radiation, slip conditions, and heat source. *AIP Adv.* **10**(1), 015038 (2020).
25. Bilal, M., Sagheer, M. & Hussain, S. Numerical study of magnetohydrodynamics and thermal radiation on Williamson nanofluid flow over a stretching cylinder with variable thermal conductivity. *Alex. Eng. J.* **57**(4), 3281–3289 (2018).
26. Gajjela, N. & Garvandha, M. The influence of magnetized couple stress heat, and mass transfer flow in a stretching cylinder with convective boundary condition, cross-diffusion, and chemical reaction. *Thermal Sci. Eng. Progress* **18**, 100517 (2020).
27. Tlili, I., Waqas, H., Almaneea, A., Khan, S. U. & Imran, M. Activation energy and second order slip in bioconvection of Oldroyd-B nanofluid over a stretching cylinder: A proposed mathematical model. *Processes* **7**(12), 914 (2019).
28. Shojaei, A., Amiri, A. J., Ardahaie, S. S., Hosseinzadeh, K. & Ganji, D. D. Hydrothermal analysis of Non-Newtonian second grade fluid flow on radiative stretching cylinder with Soret and Dufour effects. *Case Stud. Therm. Eng.* **13**, 100384 (2019).

29. Jawad, M. *et al.* Analytical study of MHD mixed convection flow for Maxwell nanofluid with variable thermal conductivity and Soret and Dufour effects. *AIP Adv.* **11**(3), 035215 (2021).
30. Ramzan, M., Bilal, M. & Chung, J. D. Soret and Dufour effects on three dimensional upper-convected Maxwell fluid with chemical reaction and non-linear radiative heat flux. *Int. J. Chem. React. Eng.* **15**(3), 20160136 (2017).
31. Sulochana, C., Payad, S. S. & Sandeep, N. Non-uniform heat source or sink effect on the flow of 3D Casson fluid in the presence of Soret and thermal radiation. *Int. J. Eng. Res. Afr.* **20**, 112–129 (2016).
32. Ramzan, M., Yousaf, F., Farooq, M. & Chung, J. D. Mixed convective viscoelastic nanofluid flow past a porous media with Soret—DuFour effects. *Commun. Theor. Phys.* **66**(1), 133 (2016).
33. Sulochana, C., Samrat, S. P. & Sandeep, N. Numerical investigation of magnetohydrodynamic (MHD) radiative flow over a rotating cone in the presence of Soret and chemical reaction. *Propuls. Power Res.* **7**(1), 91–101 (2018).
34. Sulochana, C., Samrat, S. P. & Sandeep, N. Magnetohydrodynamic radiative nanofluid flow over a rotating surface with Soret effect. *Multidiscip. Model. Mater. Struct.* **14**, 168–188 (2018).
35. El-Kabeir, S. M. M., Chamkha, A., & Rashad, A. M. Heat and mass transfer by MHD stagnation-point flow of a power-law fluid towards a stretching surface with radiation, chemical reaction and Soret and Dufour effects. *Int. J. Chem. Reactor Eng.* **8**(1) (2010).
36. Ramzan, M., Farooq, M., Hayat, T., Alsaedi, A. & Cao, J. MHD stagnation point flow by a permeable stretching cylinder with Soret-Dufour effects. *J. Cent. South Univ.* **22**(2), 707–716 (2015).
37. Chamkha, A. J., El-Kabeir, S. M. M. & Rashad, A. M. Unsteady coupled heat and mass transfer by mixed convection flow of a micropolar fluid near the stagnation point on a vertical surface in the presence of radiation and chemical reaction. *Progress Comput. Fluid Dyn.* **15**(3), 186–196 (2015).
38. Layek, G. C., Mandal, B. & Bhattacharyya, K. Dufour and Soret effects on unsteady heat and mass transfer for powell-eyring fluid flow over an expanding permeable sheet. *J. Appl. Comput. Mech.* **6**(4), 985–998 (2020).
39. Jawad, M., Saeed, A., Kumam, P., Shah, Z. & Khan, A. Analysis of boundary layer MHD darcy-forchheimer radiative nanofluid flow with Soret and Dufour effects by means of marangoni convection. *Case Stud. Therm. Eng.* **23**, 100792 (2021).
40. Ramudu, A. V., Kumar, K. A., Sugunamma, V., & Sandeep, N. Impact of Soret and Dufour on MHD Casson fluid flow past a stretching surface with convective–diffusive conditions. *J. Therm. Anal. Calorim.* (2021).
41. Jagadha, S., Gopal, D. & Kishan, N. Soret and Dufour effects of electrical MHD nanofluid with higher order chemical reaction. *Test Eng. Manag.* **82**, 2250–2259 (2020).
42. Jagan, K., Sivasankaran, S., Bhuvaneswari, M., Rajan, S. & Makinde, O. D. Soret and Dufour effect on MHD Jeffrey nanofluid flow towards a stretching cylinder with triple stratification, radiation and slip. In *Defect and diffusion forum* Vol. 387 (ed. Makinde, O. D.) 523–533 (Trans Tech Publications Ltd., 2018).
43. Kasali, K. B., Tijani, Y. O., Lawal, M. O., & Lawal, Y. T. Soret, Dufour and radiation effects of a viscoelastic fluid on an exponentially stretching surface using the Catteneo–Christov heat flux model. *Multidiscipline Model. Mater. Struct.* (2020).
44. Singh, K., Pandey, A. K. & Kumar, M. Melting heat transfer assessment on magnetic nanofluid flow past a porous stretching cylinder. *J. Egypt. Math. Soc.* **29**(1), 1–14 (2021).
45. Bisht, A. & Sharma, R. Comparative analysis of a Sisko nanofluid over a stretching cylinder through a porous medium. *Heat Transf.* **49**(6), 3477–3488 (2020).
46. Saeed, A. *et al.* Darcy-Forchheimer MHD hybrid nanofluid flow and heat transfer analysis over a porous stretching cylinder. *Coatings* **10**(4), 391 (2020).
47. Aminian, E., Moghadasi, H. & Saffari, H. Magnetic field effects on forced convection flow of a hybrid nanofluid in a cylinder filled with porous media: A numerical study. *J. Therm. Anal. Calorim.* **141**, 2019–2031 (2020).
48. Awais, M., Raja, M. A. Z., Awan, S. E., Shoaib, M. & Ali, H. M. Heat and mass transfer phenomenon for the dynamics of Casson fluid through porous medium over shrinking wall subject to Lorentz force and heat source/sink. *Alex. Eng. J.* **60**(1), 1355–1363 (2021).
49. El-Hakiem, M. A. & Rashad, A. M. Effect of radiation on non-Darcy free convection from a vertical cylinder embedded in a fluid-saturated porous medium with a temperature-dependent viscosity. *J. Porous Med.* **10**(2), 209–218 (2007).
50. Rashad, A. M. & El-Kabeir, S. M. M. Heat and mass transfer in transient flow by mixed convection boundary layer over a stretching sheet embedded in a porous medium with chemically reactive species. *J. Porous Media* **13**(1), 75–85 (2010).
51. Alwawi, F. A., Alkasasbeh, H. T., Rashad, A. M. & Idris, R. A numerical approach for the heat transfer flow of carboxymethyl cellulose-water based Casson nanofluid from a solid sphere generated by mixed convection under the influence of Lorentz force. *Mathematics* **8**(7), 1094 (2020).
52. Rashad, A. M., Chamkha, A. J. & El-Kabeir, S. M. M. Effect of chemical reaction on heat and mass transfer by mixed convection flow about a sphere in a saturated porous media. *Int. J. Numer. Methods Heat Fluid Flow* **21**, 418–433 (2011).
53. Subbarayudu, K., Suneetha, S., Reddy, P. B. A. & Rashad, A. M. Framing the activation energy and binary chemical reaction on CNT's with Cattaneo-Christov heat diffusion on maxwell nanofluid in the presence of nonlinear thermal radiation. *Arab. J. Sci. Eng.* **44**(12), 10313–10325 (2019).
54. Rashad, A. M., Chamkha, A. J. & El-Kabeir, S. M. M. Effects of radiation and chemical reaction on heat and mass transfer by natural convection in a micropolar fluid-saturated porous medium with streamwise temperature and species concentration variations. *Heat Transf. Res.* **45**(8), 795–815 (2014).
55. El-Kabeir, S. M. M., Modather, M. & Rashad, A. M. Heat and mass transfer by unsteady natural convection over a moving vertical plate embedded in a saturated porous medium with chemical reaction, Soret and Dufour effects. *J Appl. Fluid Mech.* **8**, 453–463 (2015).
56. Abbas, S. Z. *et al.* Entropy optimized Darcy-Forchheimer nanofluid (silicon dioxide, molybdenum disulfide) subject to temperature dependent viscosity. *Comput. Methods Programs Biomed.* **190**, 105363 (2020).
57. Nabwey, H. A., El-Kabeir, S. M. M. & Rashad, A. M. Lie group analysis of effects of radiation and chemical reaction on heat and mass transfer by unsteady slip flow from a non-isothermal stretching sheet immersed in a porous medium. *J. Comput. Theor. Nanosci.* **12**(11), 4056–4062 (2015).
58. Ullah, I. *et al.* MHD slip flow of Casson fluid along a nonlinear permeable stretching cylinder saturated in a porous medium with chemical reaction, viscous dissipation, and heat generation/absorption. *Symmetry* **11**(4), 531 (2019).
59. Butt, A. S., Ali, A. & Mehmood, A. Numerical investigation of magnetic field effects on entropy generation in viscous flow over a stretching cylinder embedded in a porous medium. *Energy* **99**, 237–249 (2016).
60. Wang, J., Muhammad, R., Khan, M. I., Khan, W. A. & Abbas, S. Z. Entropy optimized MHD nanomaterial flow subject to variable thicked surface. *Comput. Methods Programs Biomed.* **189**, 105311 (2020).
61. Khan, M. I., Waqas, M., Hayat, T., Khan, M. I. & Alsaedi, A. Numerical simulation of nonlinear thermal radiation and homogeneous-heterogeneous reactions in convective flow by a variable thicked surface. *J. Mol. Liq.* **246**, 259–267 (2017).
62. Khan, M. I., Waqas, M., Hayat, T. & Alsaedi, A. A comparative study of Casson fluid with homogeneous-heterogeneous reactions. *J. Colloid Interface Sci.* **498**, 85–90 (2017).
63. Khan, M. I., Hayat, T., Waqas, M. & Alsaedi, A. Outcome for chemically reactive aspect in flow of tangent hyperbolic material. *J. Mol. Liq.* **230**, 143–151 (2017).
64. Khan, M. I., Alzahrani, F. & Hobiny, A. Heat transport and nonlinear mixed convective nanomaterial slip flow of Walter-B fluid containing gyrotactic microorganisms. *Alex. Eng. J.* **59**(3), 1761–1769 (2020).

65. Ijaz Khan, M. & Alzahrani, F. Activation energy and binary chemical reaction effect in nonlinear thermal radiative stagnation point flow of Walter-B nanofluid: Numerical computations. *Int. J. Mod. Phys. B* **34**(13), 2050132 (2020).
66. Hayat, T., Ahmad, S., Khan, M. I. & Alsaedi, A. Simulation of ferromagnetic nanomaterial flow of Maxwell fluid. *Results in physics* **8**, 34–40 (2018).
67. Nayak, M. K., Shaw, S., Khan, M. I., Pandey, V. S. & Nazeer, M. Flow and thermal analysis on Darcy–Forchheimer flow of copper-water nanofluid due to a rotating disk: A static and dynamic approach. *J. Market. Res.* **9**(4), 7387–7408 (2020).
68. Farooq, M. *et al.* MHD stagnation point flow of viscoelastic nanofluid with non-linear radiation effects. *J. Mol. Liq.* **221**, 1097–1103 (2016).
69. Khan, M. I., Kumar, A., Hayat, T., Waqas, M. & Singh, R. Entropy generation in flow of Carreau nanofluid. *J. Mol. Liq.* **278**, 677–687 (2019).
70. Hayat, T. *et al.* Impact of Cattaneo-Christov heat flux model in flow of variable thermal conductivity fluid over a variable thicked surface. *Int. J. Heat Mass Transf.* **99**, 702–710 (2016).
71. Hayat, T., Khan, M. I., Farooq, M., Alsaedi, A. & Yasmeen, T. Impact of Marangoni convection in the flow of carbon–water nanofluid with thermal radiation. *Int. J. Heat Mass Transf.* **106**, 810–815 (2017).
72. Fathizadeh, M. *et al.* An effective modification of the homotopy perturbation method for MHD viscous flow over a stretching sheet. *J. King Saud Univ.-Sci.* **25**(2), 107–113 (2013).
73. Fang, T., Zhang, J. & Yao, S. Slip MHD viscous flow over a stretching sheet–an exact solution. *Commun. Nonlinear Sci. Numer. Simul.* **14**(11), 3731–3737 (2009).
74. Imtiaz, M., Hayat, T. & Alsaedi, A. Mixed convection flow of Casson nanofluid over a stretching cylinder with convective boundary conditions. *Adv. Powder Technol.* **27**(5), 2245–2256 (2016).

Author contributions

M.R. supervised and conceived the idea; N.S wrote the manuscript. H.M.A. and P.K. helped in revising the manuscript. Z.S. worked on the software and the funding arrangements.

Funding

The authors acknowledge the financial support provided by the Center of Excellence in Theoretical and Computational Science (TaCS-CoE), KMUTT". Moreover, this research project is supported by Thailand Science Research and Innovation (TSRI) Basic Research Fund: Fiscal year 2021 under project number 64A306000005.

Competing interests

The authors declare no competing interests.

Additional information

Correspondence and requests for materials should be addressed to Z.S. or P.K.

Reprints and permissions information is available at www.nature.com/reprints.

Publisher's note Springer Nature remains neutral with regard to jurisdictional claims in published maps and institutional affiliations.